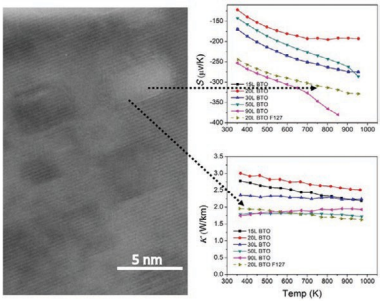

$Ba_{1-x}La_xTiO_3$ bulk thermoelectrics with rectangular nanopores is successfully fabricated by micelle assembly method using surfactant F127, followed by spark plasma sintering process. The nanoscale pores in the bulk sample significantly reduce the phonon thermal conductivity and improve the thermopower, which makes a substantial improvement of the figure of merit.

ADVANCED ELECTRONIC MATERIALS
www.advelectronicmat.de

Significant Reduction in Thermal Conductivity and Improved Thermopower of Electron-Doped $Ba_{1-x}La_xTiO_3$ with Nanostructured Rectangular Pores

Al Jumlat Ahmed, David Cortie, Frank Yun, Yasir Rahman, Sheik Md Kazi Nazrul Islam, Abdulhakim Bake, Konstantin Konstantinov, Md. Shahriar A. Hossain,* Azhar Alowasheeir, Yusuke Yamauchi, and Xiaolin Wang*

Electron-doped $BaTiO_3$ is a less studied *n*-type metal oxide thermoelectric (TE) material. In this work, the electrical conductivity of $BaTiO_3$ samples has been improved by introducing La to yield an *n*-type $Ba_{1-x}La_xTiO_3$ semiconducting material. Density functional theory calculations show that the optimal electron-doping occurs at $x = 0.2$, and this is also confirmed experimentally. To improve the TE properties further, nanostructured cuboidal pores are introduced into the bulk $Ba_{1-x}La_xTiO_3$ using F127 surfactant micelles for a chemical templating process, followed by spark plasma sintering. Interestingly, transmission electron microscopy (TEM) images reveal that the sample synthesized using the surfactant F127 has nanostructured rectangular prism pores of around 4 nm within a highly crystalline structure. X-ray powder diffraction (XRD) analysis confirms that all the La doped samples have the cubic $BaTiO_3$ perovskite phase. Scanning electron microscopy (SEM) images show that all the samples have similar grain boundaries and uniform La doping, which suggests that the large reduction in the lattice thermal conductivity in the F127-treated samples arises primarily from the pore distribution which introduces anisotropic phonon scattering within the unique nanoarchitecture. The thermal conductivity of the sample is less than 2 $W K^{-1} m^{-1}$ at room temperature, and it reduces to 1.5 $W K^{-1} m^{-1}$ at 950 K. The sample with 20 at% La doping and nanopores also shows a thermopower (Seebeck coefficient) that is doubled compared to the related sample without porosity. Together with the lattice thermal conductivity, this enables a significant improvement in the figure of merit, *zT* compared to the other samples.

1. Introduction

Metal oxide thermoelectric (TE) materials have tremendous potential for waste heat recovery from automotive exhaust systems and industrial furnaces because they are chemically stable at high temperatures, and also offer robust physical properties.[1] The performance of TE materials is assessed by the dimensionless figure of merit, $zT = \frac{S^2\sigma}{\kappa} T$, where, S, σ, T, and κ are the Seebeck coefficient which is also known as the thermo-power, the electrical conductivity, the absolute temperature, and the thermal conductivity respectively.[2–5] The term $S^2\sigma$ is called the power factor of the TE material.

Barium titanate ($BaTiO_3$) is a very well-studied material and is very popular as a lead-free ferroelectric (piezoelectric) material.[6] The perovskite crystal structure of $BaTiO_3$ changes with temperature. Above the Curie temperature (120 °C), it has a cubic crystal structure. Below the Curie temperature which lies near ambient temperatures (120 to 5 °C), one axis (the *c* axis) stretches, while the other two axes shrink, as the crystal structure

A. J. Ahmed, D. Cortie, F. Yun, Y. Rahman, A. Bake, K. Konstantinov, M. S. A. Hossain, X. Wang
Institute for Superconducting and Electronic Materials (ISEM)
Australian Institute of Innovative Materials (AIIM)
University of Wollongong
North Wollongong, NSW 2500, Australia
E-mail: md.hossain@uq.edu.au; xiaolin@uow.edu.au

S. M. K. N. Islam
School of Mathematical and Physical Sciences
University of Technology Sydney
Sydney, NSW 2007, Australia

The ORCID identification number(s) for the author(s) of this article can be found under https://doi.org/10.1002/aelm.202001044.

DOI: 10.1002/aelm.202001044

M. S. A. Hossain, Y. Yamauchi
Australian Institute for Bioengineering and Nanotechnology (AIBN)
The University of Queensland
Brisbane, QLD 4072, Australia
M. S. A. Hossain
School of Mechanical and Mining Engineering, Faculty of Engineering
Architecture and Information Technology (EAIT)
University of Queensland
St Lucia, QLD 4072, Australia

A. Alowasheeir
International Research Center for Materials Nanoarchitechtonics (WPI-MANA)
National Institute for Materials Science (NIMS)
1-1 Namiki, Tsukuba, Ibaraki 305-0044, Japan

becomes tetragonal. Above the Curie temperature, $BaTiO_3$ does not show any piezoelectric effect due to its cubic perovskite structure. However, it has a similar cubic perovskite structure like $SrTiO_3$ above the Curie temperature, but its TE properties are not well studied.[7,8] A previous theoretical study compares the TE properties of $SrTiO_3$ and $BaTiO_3$. The study describes that due to the higher lattice constant (4.060 Å) of $BaTiO_3$ compare to $SrTiO_3$ (3.928 Å), the $BaTiO_3$ has a lower electrical conductivity but a higher Seebeck coefficient in terms of carrier concentration.[7] The intrinsic thermal conductivity at room temperature of $BaTiO_3$ is also low (6 W K^{-1} m^{-1}) compared to $SrTiO_3$ (12 W K^{-1} m^{-1}). These points indicate that the $BaTiO_3$ could be a potentially useful TE oxide material.

Some experimental studies were also done on the TE properties of $BaTiO_3$. TE properties of Fe doped $BaTiO_3$ were reported at high temperatures.[9] The XRD results show the crystal structures of Fe doped $BaTiO_3$ are mixtures of tetragonal and cubic perovskite $BaTiO_3$ phases. The electrical conductivity increases with temperature and Fe concentration because of the substitution of Ti^{4+} with Fe^{3+} which also increases the oxygen vacancy population. The power factor also increases with temperature and Fe concentration. The mixed structure of crystalline phases has good potential for enhancing the TE properties.[9]

In another study, barium titanate and graphene oxide composites were prepared by the spark plasma sintering (SPS) technique containing graphene oxide up to 4 weight%. The maximum zT value of 0.008 at 550 K was achieved in the sample with 1.7 w% of graphene oxide.[10] In related work, it was reported that the Eu substitution in reduced $Ba_{1-x}Eu_xTiO_{3-\delta}$ slightly decreases the Seebeck coefficient and enhances the thermal conductivity. But it improves the electrical conductivity significantly by introducing new electronic states in the bandgap, near the band-edge. The sample $Ba_{1-x}Eu_xTiO_{3-\delta}$, x = 0.9 shows a zT of 0.25 at 1100 K.[11] Following on this theme, the TE properties of La doped $SrTiO_3$-$BaTiO_3$ solid solutions have been studied for different levels of Sr substitution. The electrical conductivity increases, but the Seebeck coefficient decreases with increasing Sr concentration, which is related to the lattice parameter. The latter result indicates that a shorter Ti-Ti distance is desirable for improvement in the power factor. The thermal conductivity increases with Sr concentration which disagrees with the point defect scattering theory.[12] Conducting polyaniline (PANI) and $BaTiO_3$ nanoparticle composite films have also been investigated for TE properties.[13] The composite film behaves like a p-type TE material. The electrical conductivity is improved compared to pure $BaTiO_3$, but the Seebeck coefficient recedes. Therefore, there is no significant improvement in the power factor of conducting PANI and $BaTiO_3$ nanoparticle composite films. In another study, lead magnesium-niobate $Pb(Mg_{1/3}Nb_{2/3})O_3$ (PMN) has been incorporated in different contents with pure $BaTiO_3$ to improve its TE efficiency by increasing the degree of A and B site disordering by Pb^{2+} and $(Mg, Nb)^{4+}$ ions. It shows that by increasing the contents of PMN, the electrical conductivity increases, and the thermal conductivity decreases. Therefore, there is an overall improvement in the TE performance of PMN incorporated $BaTiO_3$.[14] Complex double perovskites $Ba_xSr_{1-x}TiFeO_6$ with $0.0 \leq x \geq 0.25$ show p-type TE behavior and the sample with $x = 0.25$ shows very high thermo-power of 800 μV K^{-1} at 1123K.[15] On the other hand, Niobium doped barium titanate ($BaNb_xTi_{1-x}O_3$) exhibits n-type TE behavior whose electrical conductivity is directly proportional to the temperature.[16] Yttrium doped n-type $BaTiO_3$ shows a thermo-power of −550 μV K^{-1} at 350 K.[17]

Previously, we have reported that La doping optimization and nanostructured porosity into bulk material can improve the TE properties of $SrTiO_3$.[18,19] $BaTiO_3$ has a similar cubic perovskite structure above the Curie temperature. It has intrinsically low thermal conductivity and chemical stability at high temperatures. Its electrical conductivity can be changed easily by electron doping. Electron doped $BaTiO_3$ was reported as a TE material though it exhibited a low figure of merit such as zT value of 0.008 at 550 K.[10] It was also reported that its transport properties like electrical conductivity and Seebeck coefficient can be improved by doping optimization.[7,11,14] However so far, no research has been done to reduce the thermal conductivity which can improve its TE performance. Here we report for the first time that the thermal conductivity of $BaTiO_3$ can be suppressed and the Seebeck coefficient can be improved greatly by introducing nanostructured pores into the bulk sample. The main objective of our research is to examine the effect of nanostructured pores on TE properties of $BaTiO_3$ which is intrinsically an insulating material. Therefore, the electrical conductivity is improved, and it becomes n-type semiconducting material because of electron doping by adding La in atomic percentage.

2. Results and Discussion

2.1. Density Functional Theory (DFT) Calculations

Figure 1 shows the total density of states (TDOS) and the contribution of electrons from s, p, and d orbitals to the DOS for undoped (Figure 1a) and La doped $BaTiO_3$. Different doping levels are considered by varying the amount of La yielding cells including: $La_{0.25}Ba_{0.75}TiO_3$, $La_{0.5}Ba_{0.5}TiO_3$, and $La_{0.75}Ba_{0.25}TiO_3$ as shown in Figure 1b–d. For all cases, the electrons of p orbital are the majority contributor of the valence band and electrons of d orbital are the majority contributor of the conduction band. The Fermi level shifts into the conduction band as shown in Figure 1b for 25 at% La doping and the material becomes an n-type semiconductor with improved electrical conductivity. However, for 50 and 75 at% La doping, there is no further increment in the DOS at the Fermi level and the bandgap only increases slightly as shown in Figure 1c,d respectively. The band structures of supercell for bare sample $Ba_8Ti_8O_{24}$ and 25 at% La added sample $Ba_6La_2Ti_8O_{24}$ are available in Figure S2 a,b,

Y. Yamauchi
JST-ERATO Yamauchi Materials Space-Tectonics Project and
International Center for Materials Nanoarchitectonics (WPI-MANA)
National Institute for Materials Science (NIMS)
1-1 Namiki, Tsukuba, Ibaraki 305-0044, Japan
Y. Yamauchi
School of Chemical Engineering
Faculty of Engineering
Architecture and Information Technology (EAIT)
University of Queensland
St Lucia, QLD 4072, Australia

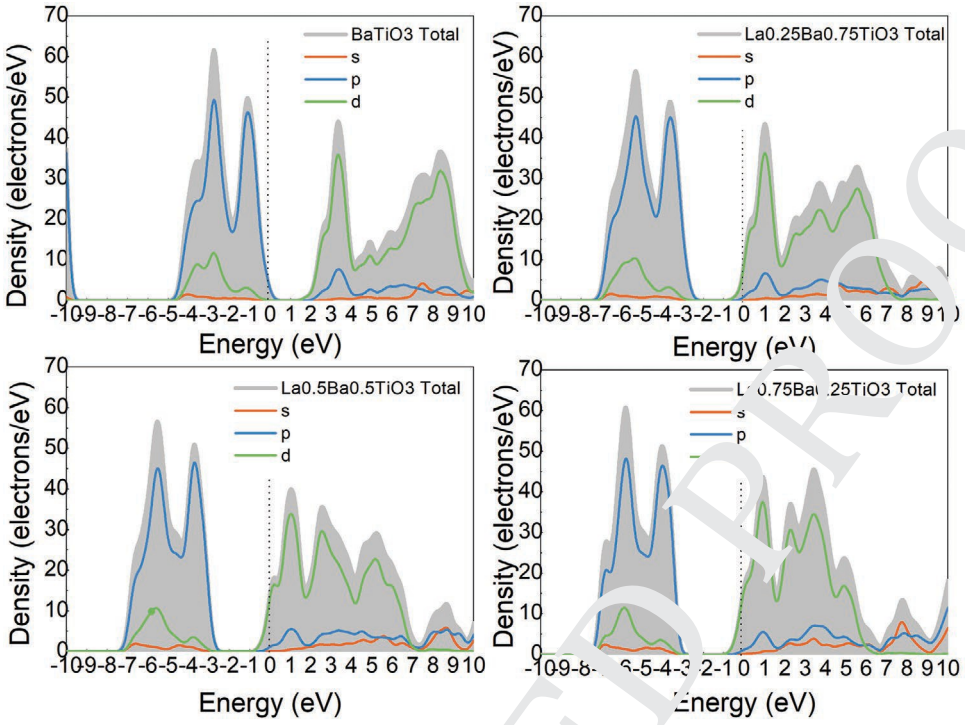

Figure 1. The density of state (DOS) of $BaTiO_3$ samples with different La doping a) bare, b) 25 at% La, c) 50 at% La and d) 75 at% La doped $BaTiO_3$.

Supporting Information. The band structures show that the Fermi level shifts toward the conduction band due to 25 at% La doping which means the doped sample becomes an *n*-type semiconductor and the energy bandgap reduces to 1.8 eV. This finding predicts that the electrical conductivity is increased by moderate La-doping which results in an *n*-type semiconductor, but higher doping levels will not result in any additional enhancement in the conductivity.

2.2. Experimental Results

The X-ray diffraction (XRD) patterns of La doped $BaTiO_3$ powder samples calcinated at 600 °C are shown in Figure S1, Supporting Information. All the samples were measured by the same instrument. The calcinated powder samples with and without La doping have the cubic $BaTiO_3$ phase (JCPDS data No. 31–0174).[20] The (200) peaks located at 45° are marked with a dotted box. It is interesting to observe that the sample 20L BTO F127 prepared with 600 mg of surfactant F127 shows more obvious XRD peaks, compared to other samples prepared without surfactant F127. The average crystallite size of the samples was calculated from the XRD peaks using Scherrer's equation. The calculations show that samples with and without surfactant F127 have an average crystallite size of around 20 nm. It suggests that the crystallite size of the sample with surfactant F127 does not change due to the presence of nanoscale pores.

The XRD patterns of the La doped $BaTiO_3$ bulk samples synthesized by SPS are shown in **Figure 2**a-1. The overall synthesis process including the SPS step is shown in Figure S3, Supporting Information. The XRD patterns confirm that the primary phase is cubic $BaTiO_3$, since there is a single peak at around 45°. The same general features are observed in the XRD patterns of the starting powder samples (Figure S1, Supporting Information) prior to sintering. In Figure 2a-2, the gradual shift toward higher diffraction angles of the enlarged (110) peak proves that the La doping into the lattice of $BaTiO_3$ causes substitution and lattice contraction. The gradual reduction in the lattice parameter with an increasing La doping indicates that Ba atoms on the A sites of the ABO_3 crystal system are replaced by La since La (217 pm) has a smaller atomic radius than the Ba (253 pm) as shown in Figure 2b.

The 20L BTO F127 sample was prepared by adding the surfactant F127 during the powder preparation (Figure S3, Supporting Information). During the solution preparation, the inorganic species accumulate around the micelles. The solution is dispensed into filter paper and is kept at 600 °C for calcination. During calcination, the crystal formation of the frameworks starts around the micelles and the micelles are removed within the crystal at high temperature. In **Figure 3**, the nitrogen gas adsorption-desorption isotherm, pore size distribution curve, and the transmission electron microscopy (TEM) images of the sample (20L BTO F127) confirm the presence of nanostructured pores. In Figure 3a, a gradual uptake of nitrogen gas in the adsorption range indicates that the resulting pore sizes are random. The pore size distribution curve (Figure 3b) shows the pore sizes are distributed in the range from 2 to 16 nm, with the majority of pores having diameters of 4 nm. The TEM images (Figure 3c,d) give localized information on the existence of nanostructured pores of size from 3 to 7 nm where the majority pores are around 4 nm which is in line with the pore size distribution result. The presence of lattice fringes in the TEM indicates that the pores are formed within crystalline

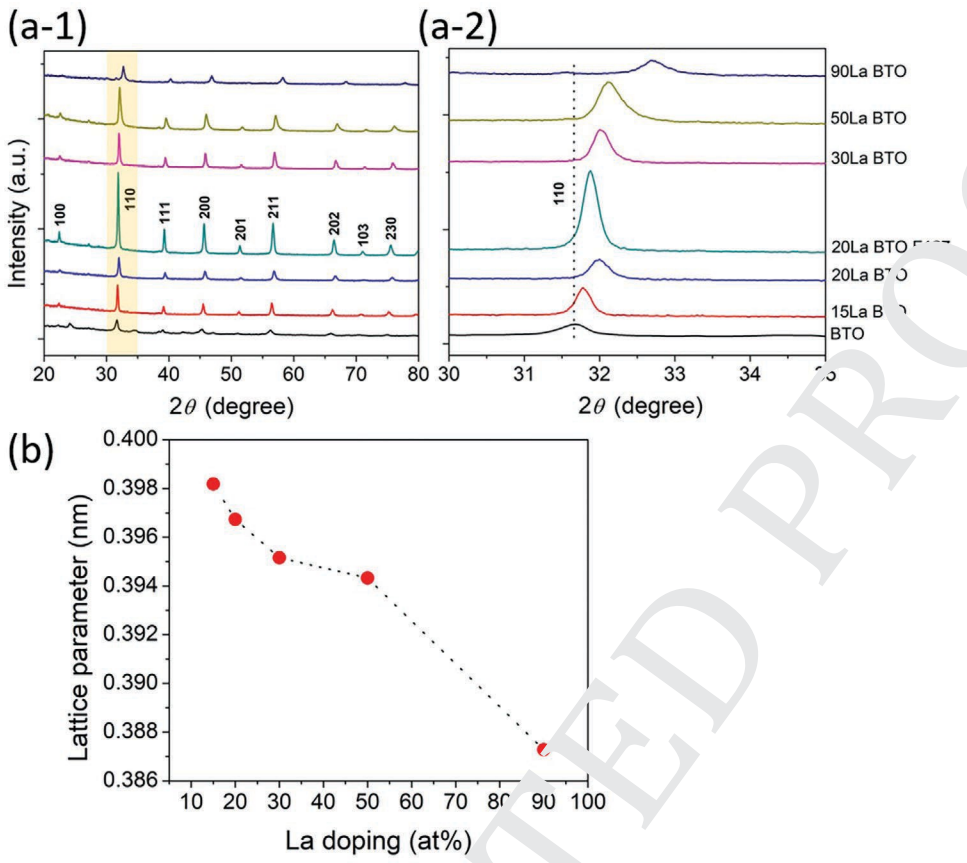

Figure 2. a-1) XRD pattens of $BaTiO_3$ bulk samples with different atomic percentage of La doping, a-2) the enlargered peak (110) shows the peak shifting with La doping and b) lattice parameter with La doping in atomic percentage.

grains and most of the pores are rectangular in shape. The TEM images also show that the distance between pores is a few nanometers. In contrast, the TEM images (Figure 3e,f) of the sample without surfactant F127 (20L BTO) reveal the absence of nanoscale pores within the crystalline grain. The lattice fringes in Figure 3e confirm the well-developed crystallinity of the sample. The above results provide direct evidence that the sample 22L BTO F127 has nanostructured pores due to the use of the surfactant F127.

Generally, the resulting pore shapes depend on the shape of the used micelles. Mesoporous/nanoporous materials prepared by soft-templating methods have shown spherical- or tubular-shaped pores with curvatures. In our experiments, the porous powders were densified at high temperature (1150 °C) and high pressure (70 MPa) within a short period of time using SPS. It can be suspected that during the first sintering process, the nano crystallization takes place, and the pores end up in a rectangular shape. The theoretical studies show that the phonon thermal conductivity in nanostructured material depends on pore shape and dimension.[21,22] The computational results show that the nanostructured material with square shape pores has low phonon thermal conductivity compared to circular shape pores because pores with sharp edges can scatter phonons more effectively.[23]

The nanostructure of the samples without surfactant (20L BTO) and with surfactant (20L BTO F127) are compared in **Figure 4**a,b. The Scanning electron microscopy (SEM) images of the samples show that both have a similar grain size of a few hundred nanometres. The size of some grains is indicated in the figures. The grain boundaries of both the samples are also similar. The EDS spectra in Figure 4c,d show that both the samples have the same elemental composition. The unlabeled peaks in the EDS spectra are due to Pt coating over the samples. The EDS maps in the inset of Figure 4(c(i,ii),d(i,ii)) show the spatial distribution of Ba and La is uniform in both samples. It is clear from the SEM image and EDS maps that the contribution of grain boundaries and point defects to the lattice thermal conductivity would be similar for both samples, with and without surfactant. It is therefore expected that, for the sample 20L BTO F127, the nanostructured cuboidal pores would be the main additional mechanism to reduce the lattice thermal conductivity and enhanced the power factor, although the pores may also hinder the electrical conductivity of the sample slightly.

The electrical conductivity of all the samples increases with measurement temperature which is typical of semiconducting behavior as shown in **Figure 5**a. The electrical conductivity of the sample 20L BTO is significantly higher compared to other samples. This indicates that the carrier concentration and mobility of the sample 20L BTO are in an optimum doping region, and further La-doping does not provide additional benefits. This is consistent with the predictions from the DFT

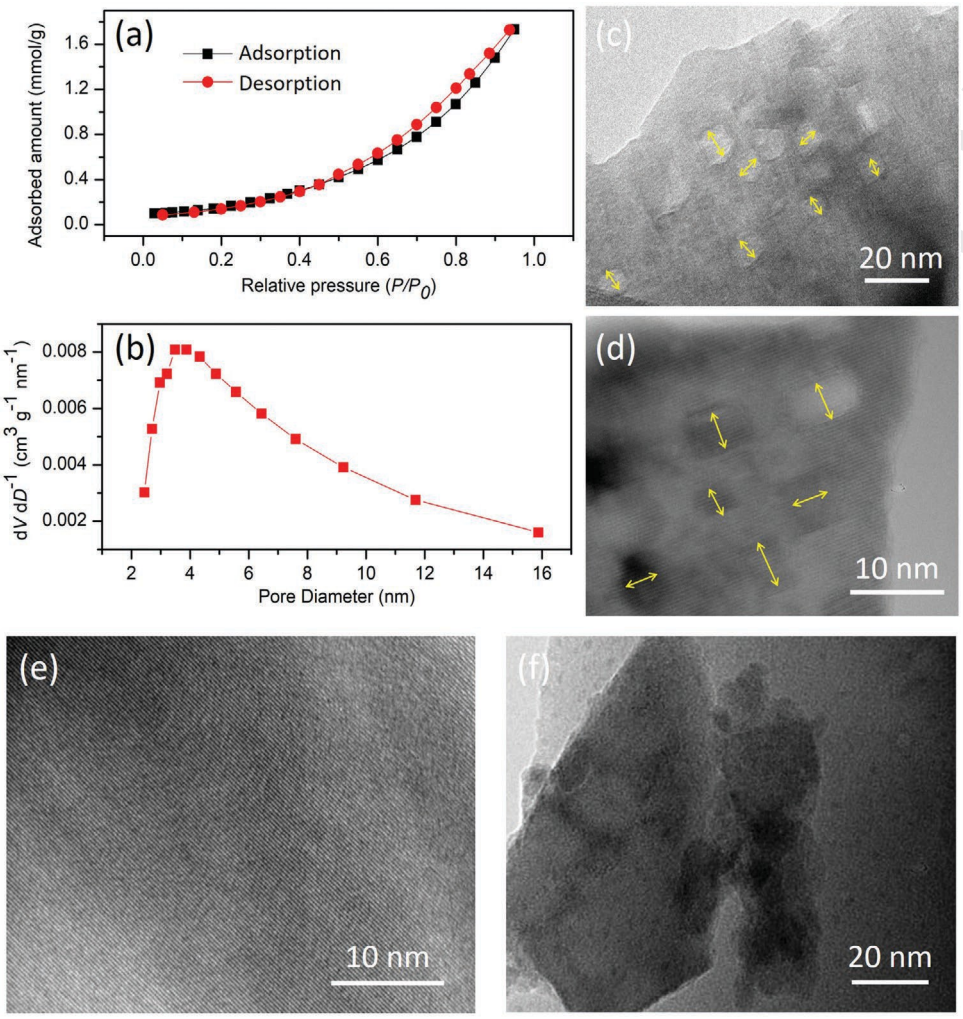

Figure 3. a) Nitrogen gas absorption-desorption isotherms, b) pore size distribution curve, and c,d) TEM images of 20L BTO F127 sample with nano-structured cuboidal pores. e,f) TEM images of 20L BTO sample without nano scale porosity.

calculations in the earlier section where the DOS calculations suggest that the electrical conductivity improves for 25 at% La doping, but it does not increase further for 50 and 75 a% doping. It is observed that there is no improvement in the electrical conductivity of $BaTiO_3$ samples for the addition of La in more than 20 atomic percentages. The addition of La to $BaTiO_3$ in more than 25 atomic percentage may be considered as alloying and since $LaTiO_3$ itself a Mott insulator, it reduces the electrical conductivity when it is in alloy form. As we know, the electrical conductivity is linearly proportional to the carrier concentration and the carrier mobility, $\sigma = n\,e\,\mu$, where e is the charge of the electron, n is the carrier concentration, and μ is the carrier mobility. The Hall effect measurement is desirable to separately measure carrier concentration and mobility, but Hall measurements of the samples are not possible due to their low conductivity. The electrical conductivity of the sample 20L BTO F127 is reduced compared to the sample 20L BTO which has the same La doping. This reduction in conductivity is due to the nanostructured pores which hinder the carrier mobility.[24] The main objective of our research was to examine the effect of nanostructured pores on TE properties of $BaTiO_3$ which is intrinsically an insulating material. Therefore, the electrical conductivity was improved, and it became n-type semiconducting material because of electron doping by adding La in atomic percentage. The electrical conductivity of $BaTiO_3$ can be improved further by using different dopants which were already reported in the literature.[7,11,14]

The value of the thermopower or Seebeck coefficient of all the samples is negative which means the samples become n-type semiconductors after doping. The Seebeck coefficient increases with temperature as shown in Figure 5b. The sample 20L BTO has the lowest thermopower compared to the other samples. This is logical because the Seebeck coefficient for the doped semiconductor is inversely related to the carrier concentration which can be expressed as $S = \frac{8\pi^2 k_B^2}{3eh^2} m^* T \left(\frac{\pi}{3n}\right)^{2/3}$, where, k_B stands for the Boltzmann constant, e for electron charge, h refers to Planck's constant, m^* refers to the effective mass of the carrier, T is the absolute temperature, and n is the carrier concentration. There is a huge improvement in the thermopower of the nano-porous sample. The thermopower is doubled for the 20L BTO F127 compared to the sample with the

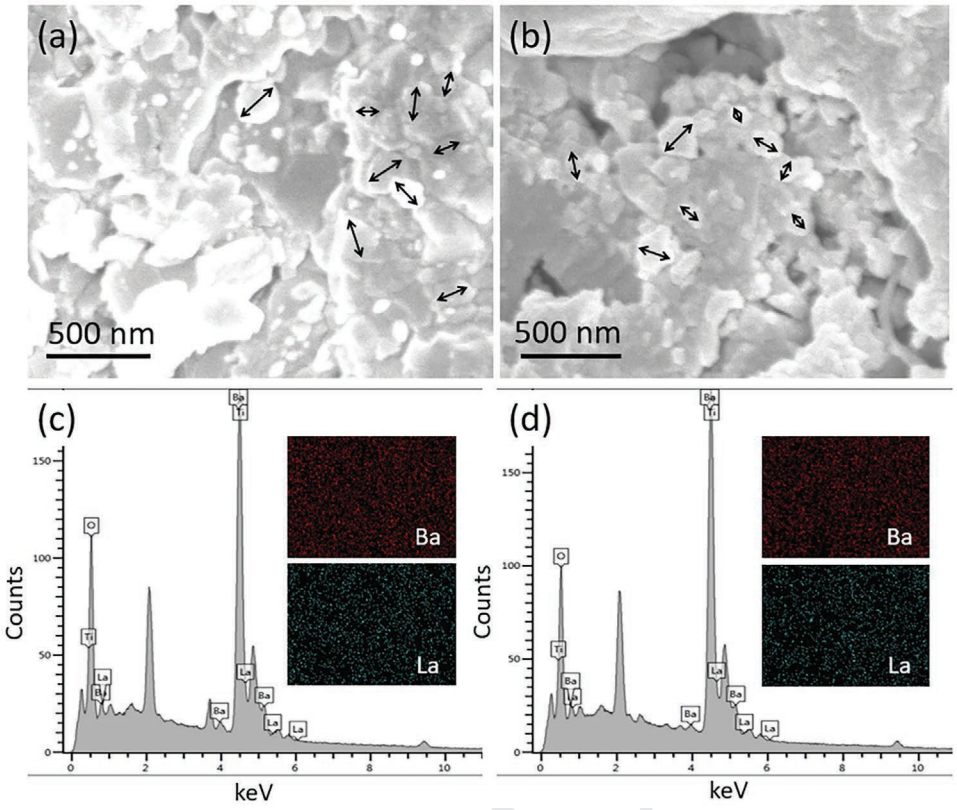

Figure 4. SE-SEM images show grain size and grain boundaries of samples. a) 20L BTO and b) 20L BTO F127. The EDS spectra show elemental composition of samples c) 20L BTO and d) 20L BTO F127. The inset figures (i) and (ii) show the distribution of Ba and La in the samples, respectively.

same doping level, but without pores, 20L BTO. The Seebeck coefficient depends on different factors like carrier concentration, diffusion of charge carrier, and carrier phonon interaction. There is an improvement in the Seebeck coefficient of the sample with nanoscale pores though it has the same 20 at% La doping as the other sample 20L BTO without pores. It indicates that the carrier concentration is not the factor for improvement of the Seebeck coefficient. Other factors such as diffusion of charge carrier due to temperature gradient and carrier phonon interaction can be responsible for the improvement of the Seebeck coefficient. It is suspected that the nanoscale pores are working as a barrier for charge carrier diffusion from the hot side toward the cold side. In addition, the scattering of phonon from nanoscale pores may change the phonon carrier interaction which can be also responsible for the improvement of the Seebeck coefficient.

Since the electrical conductivity of 20L BTO reduces due to pores but its thermopower increases significantly, the power factor of the sample is marginally higher than the sample 20L BTO. For the sample 20L BTO F127, the maximum value of the power factor is 16 $\mu W\ K^{-2}m$ at 950 K as shown in Figure 5c.

The thermal conductivity of all the samples decreases with temperature as shown in Figure 5d. The sample 20L BTO has the highest thermal conductivity. It can be observed that there is significant decay in the thermal conductivity of the samples 50L BTO and 90L BTO and this is most likely due to charge compensation of the defects in the crystal structure surrounding the La atoms which leads to a reduction in the electronic conductivity. Most importantly, however, the thermal conductivity of the sample with nanostructured pores (20L BTO F127) is remarkably reduced compared to sample 20L BTO which has the same at% of La doping but without nano porosity. This is attributed to the phonon boundary scattering by the nanostructured pores of the sample in addition to phonon defect scattering by the La atoms.[25,26] Several theoretical studies have shown that structures with pores in the range of a few nanometres to few tens of nanometres can effectively scatter phonons of different wavelengths.[27] The thermal conductivity for the nano-porous sample is less than 2 $W\ K^{-1}\ m^{-1}$ at room temperature and it is close to 1.5 $W\ K^{-1}\ m^{-1}$ at 950 K.

The thermal conductivity can be divided into two parts, κ_{el} which is the thermal conductivity due to the movement of electrons or holes, and κ_{ph} which is the thermal conduction by lattice vibration also known as the phonon thermal conductivity. Phonon thermal conductivities and electrical thermal conductivities for each temperature are shown in **Figure 6**a,b respectively. The κ_{ph} can be express as, $\kappa_{ph} = \frac{1}{3} C_v V l$, where the heat capacity (C_v) at constant volume and the phonon velocity (V) are constant, therefore, the κ_{ph} mainly relies on the phonon mean free path (MFP) (l). The mean free path of phonons in $BaTiO_3$ is on the order of 10^{-8} m which is close to the nanometer scale. So, it is possible to scatter the phonon with nanoscale pores.[28]

The mean free path of the phonons gets reduced due to the nanostructured pores in the sample 20L BTO F127, and this leads to a very low phonon thermal conductivity. To isolate the

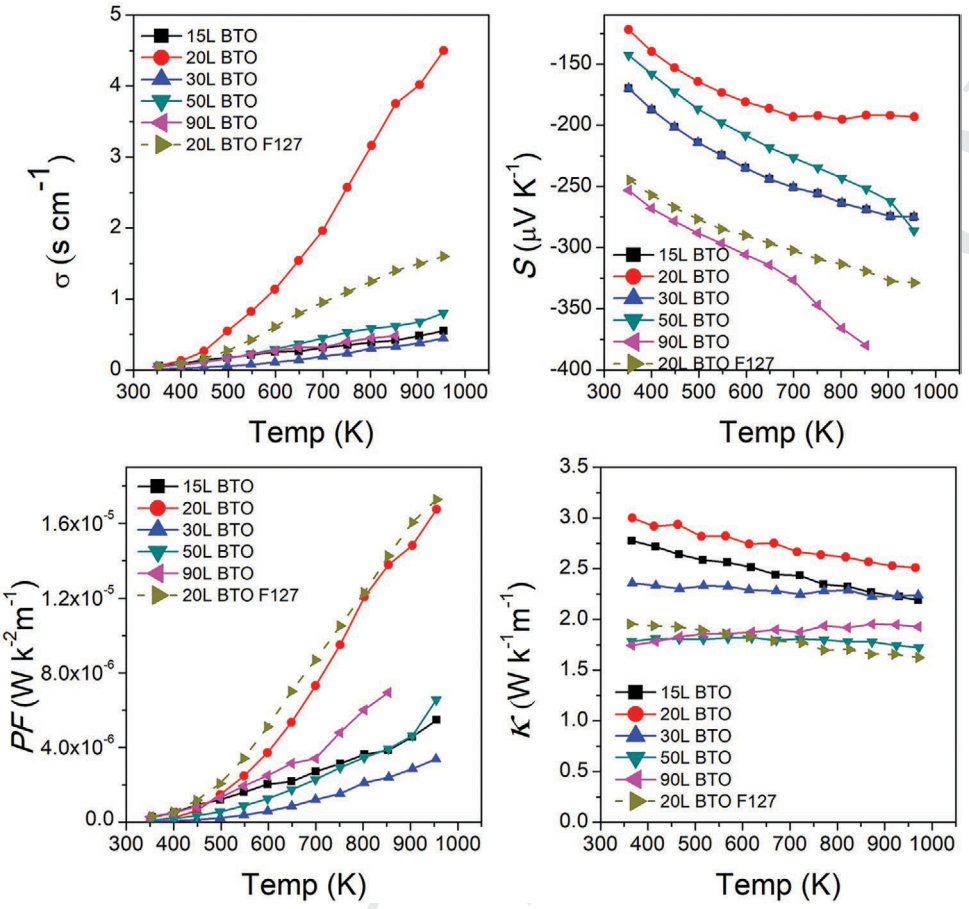

Figure 5. Transport properties of the samples as a function of temperature a) electrical conductivity σ (s cm^{-1}), b) Seebeck coefficient S (μV K^{-1}), c) Power factor PF (W K^{-2} m^{-1}), and d) Thermal conductivity κ (W K^{-1} m^{-1}).

role of the phonon thermal conductivity, the electronic contribution must first be subtracted. From the Wiedemann–Franz law, the κ_{el} is directly proportional to the electrical conductivity, σ, and temperature, T. $\kappa_{el} = LT\sigma$, where L is the proportional constant known as the Lorenz number which is an experimental value. Normally, L is treated as a universal factor with the value of 2.44×10^{-8} WΩ K^{-2} for a degenerate semiconductor. In the samples of La-doped $BaTiO_3$, the calculations show that the contribution of κ_{el} to the total thermal conductivity is insignificant. The experimental thermal conductivity is determined from the thermal diffusivity, specific heat capacity, and density of the material, $\kappa = \alpha C_p \rho$, where α, C_p, and ρ are the thermal diffusivity, heat capacity at constant pressure, and the material density, respectively. Figure 6c,d shows thermal diffusivity and the specific heat capacity of the samples. The thermal diffusivity is a measurement of the rate of heat transfer through the material. The heat transfer in the sample 20L BTO F127 is significantly lower compared to the sample 20L BTO and this may be due to the obstacles introduced by the nanostructured pores. The specific heat capacity is also lower for the sample 20L BTO F127 than others. The value of the specific heat capacity for the samples is close to the theoretical value and it is almost flat with temperature.

The nanoscale pores in the sample 20L BTO F127 reduce its electrical conductivity to some extent. However, the improvement of its thermopower is remarkable because of nanoscale pores. Additionally, the thermal conductivity of the sample is ultra-low. Therefore, there is a significant improvement in the figure of merit of the sample 20L BTO F127 as shown in **Figure 7**. The figure of merit could be improved further by optimizing the electron doping and retaining the nanoscale porosity in the sample.

3. Conclusion

The electrical conductivity of $BaTiO_3$ has been improved by optimizing the doping of La in atomic percentages and causing the samples to become n-type semiconductor materials. For further improvement of transport properties, a nanoporous architecture has been introduced in the sample 20L BTO F127 using the F127 surfactant during the powder synthesis process. The thermopower of the sample has been enhanced to more than double compare to the sample without porosity (20L BTO). The main achievement of the experiments is the suppression of the phonon propagation by nanostructured rectangular-prismatic pores which lead to a very low phonon thermal conductivity of 1.5 W K^{-1} m^{-1} at 950K in the sample 20L BTO F127. There is a reduction in the electrical conductivity of the sample 20L BTO F127 due to the nanoscale pores. However, the improvement of

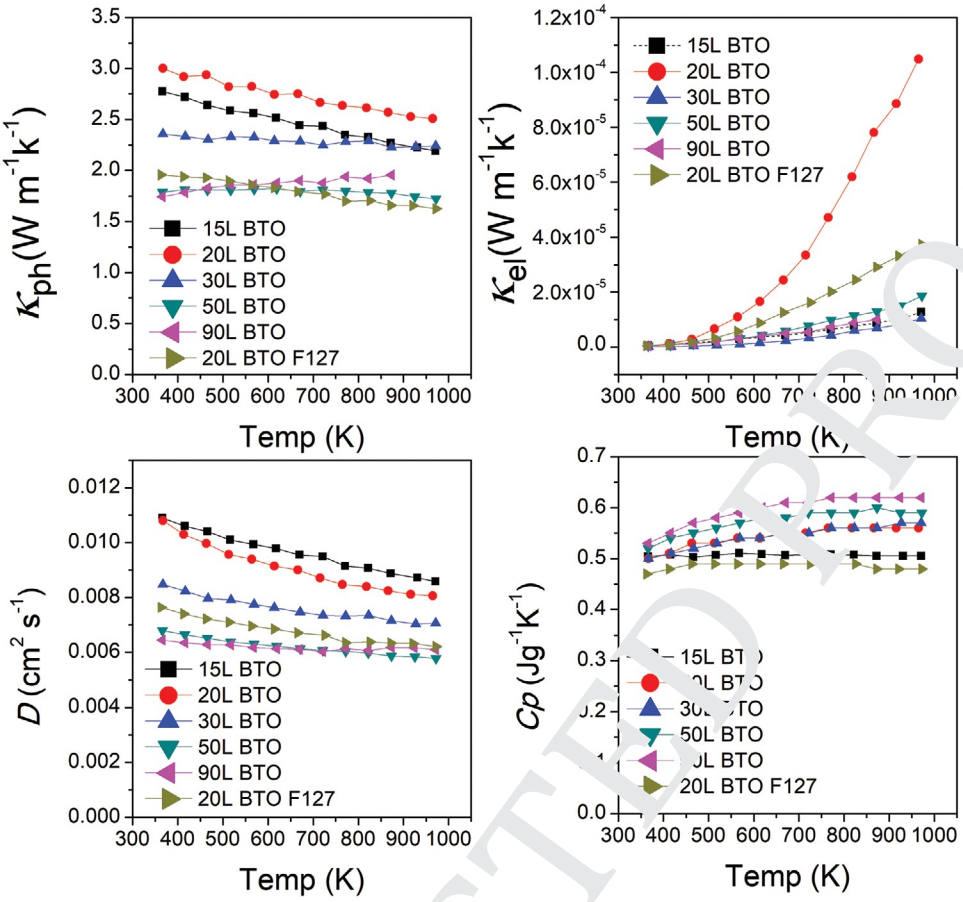

Figure 6. a) Phonon thermal conductivity κ_{ph} (W m^{-1} k^{-1}), b) electrical thermal conductivity κ_{el} (W m^{-1} k^{-1}), c) thermal diffusivity D (cm^2 s^{-1}), and d) Specific heat capacity Cp (J g^{-1} K^{-1}).

thermopower is more significant than the reduction of electrical conductivity. Therefore, the power factor of the sample 20L BTO F127 is higher than the sample without porosity 20L BTO. In addition, the reduction of thermal conductivity is remarkable because of nanoscale pores in the sample 20L BTO F127. The theoretical studies showed that the reduction in thermal conductivity is more prominent than the reduction in electrical conductivity because of nanoscale porosity and it leads to an overall improvement in the figure of merit.[29,30] This promising novel strategy of suppressing phonon thermal conductivity can be applied to other TE materials also to improve the figure of merit.

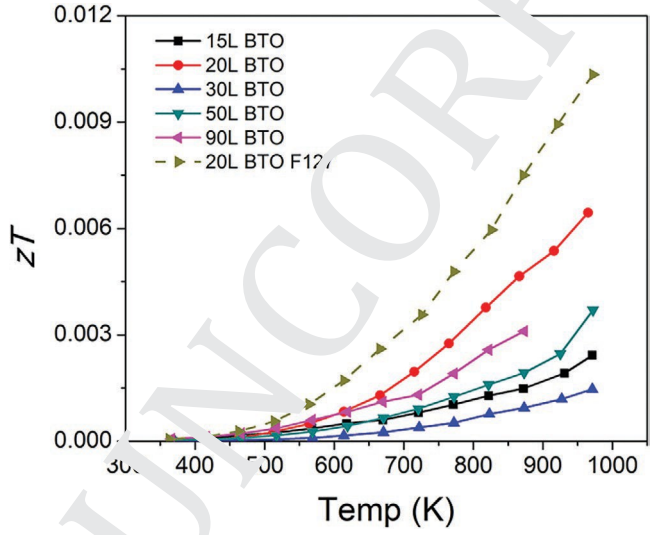

Figure 7. Figure of merit zT of the $BaTiO_3$ samples with temperature.

4. Experimental Section

Calculation Details: Density functional theory (DFT) was implemented using the CASTEP package.[31] The exchange-correlation function used to describe the exchange-correlation interaction was the General Gradient Approximation (GGA) with the Perdew–Burke–Ernzerhof (PBE) formulation,[32] with an ultra-soft pseudopotential. Atomic positions of the crystal structures were optimized using the Broyden–Fletcher–Goldfarb–Shanno algorithm.[33] The Maximum cut off energy used was 630 eV with a $4 \times 4 \times 4$ k-point set for optimizations to less than 5.0×10^{-6} eV atom^{-1}. The DOS calculation was performed using a $25 \times 25 \times 25$ k-point mesh.

Sample Preparation: To synthesis La doped $BaTiO_3$ powder, Barium acetate and lanthanum acetate hydrate were dissolved in different ratios into Acetic acid at 50 °C, and then titanium butoxide was further added into the solution at room temperature. The solution was transferred into filter paper for calcination at 600 °C for 10 min for powder preparation.

Table 1. Sintering parameters for $BaTiO_3$ in spark plasma sintering (SPS).

Temperature [°C]	Heating rate [°C min^{-1}]	Pressure [MPa]	Sintering period [min]	Relative density [%]	Ref.
750	200	50	3	94	[34]
900				99	
1100	50	80	1		[10]
950	100	75	5		[35]
975				96	
1000				99	
1025				99	
1050				99	

The process has been illustrated in Figure S3, Supporting Information. The La doped samples were symbolized after the amount of doping into $BaTiO_3$ like ($Ba_{1-x}La_xTiO_3$ (x = 0.15, 0.20, 0.30, 0.50, and 0.90)) 15L BTO, 20L BTO, 30L BTO, 50L BTO, and 90L BTO.

To introduce nanostructured porosity in La doped $BaTiO_3$ sample, the commercially available triblock copolymer (F127) was dissolved into ethanol. This solution was mixed properly with the above-mentioned La doped $BaTiO_3$ solution and then it was transferred into filter paper for calcination at 600 °C for 10 min for powder preparation. The synthesis protocol of powders with nano-scale porosity was already discussed in detail in a previous publication.[18] The sample was denoted as 20L BTO F127 based on La doping amount (20 at%) and the name of the surfactant, F127.

The powder samples were transformed into bulk samples using the SPS process. The sintering parameters for SPS to fabricate bulk samples from the nanoporous powder were selected based on published works listed in **Table 1**. The relative density of all the samples was above 90%. The applied temperature, pressure, and period were 1150 °C, 70 MPa, and 15 min sintering time.

Sample Characterization: The powder XRD patterns were determined by the X-ray diffractometry (Cu Kα, GBC MMA, λ = 1.5418 Å) with a step size of 0.02° and speed of 2° per min from 25° to 80°. The nanostructures and EDS mapping of the polished surface of samples were studied using field emission scanning electron microscopy (FE-SEM, JEOL 7500F) with a maximum magnification of ×1 000 000 and the highest resolution of 1nm. TEM images were captured in the instrument JEOL2010 ARM. The thermopower (Seebeck coefficient), S, and the electrical conductivity, σ were measured from room temperature to 950 K under vacuum using Ozawa RZ2001i. The thermal diffusivity of the samples was measured under vacuum conditions using the instrument, LINSEIS LFA 1000, and the specific heat was measured under argon atmosphere by DSC-204F1 Phoenix. The weight and dimensions of a rectangular sample were used to determine the sample density. The results of the samples were confirmed by repeating all the measurements several times.

Supporting Information

Supporting Information is available from the Wiley Online Library or from the author.

Acknowledgements

The Ph.D. scholarship of the first author, A.J.A. was funded by the prestigious Endeavour Leadership Program of the Australian Government. The authors acknowledge the contribution of Tony Romeo at the UOW Electron Microscopy Centre. The authors also acknowledge the use of the JEOL 7500 SEM, and the JEOL2010 ARM at the UOW Electron Microscopy Centre.

Conflict of Interest

The authors declare no conflict of interest.

Data Availability Statement

The data that support the findings of this study are available from the corresponding author upon reasonable request.

Keywords

La doped $BaTiO_3$, low phonon thermal conductivity, nanostructured porosity, thermopower

Received: October 27, 2020
Revised: January 28, 2021
Published online:

[1] L. M. Daniels, S. Ling, S. N. Savvin, M. J. Pitcher, M. S. Dyer, J. B. Claridge, B. Slater, F. Corà, J. Alaria, M. J. Rosseinsky, *J. Mater. Chem. A* **2018**, *6*, 15640.
[2] J. R. Sootsman, D. Y. Chung, M. G. Kanatzidis, *Angew. Chem., Int. Ed.* **2009**, *48*, 8616.
[3] Y. Yin, B. Tudu, A. Tiwari, *Vacuum* **2017**, *146*, 356.
[4] G. J. Snyder, E. S. Toberer, *Nat. Mater.* **2008**, *7*, 105.
[5] L. Zhao, S. M. K. N. Islam, J. Wang, D. L. Cortie, X. Wang, Z. Cheng, J. Wang, N. Ye, S. Dou, X. Shi, L. Chen, G. J. Snyder, X. Wang, *Nano Energy* **2017**, *41*, 164.
[6] N. Suzuki, X. Jiang, R. R. Salunkhe, M. Osada, Y. Yamauchi, *Chem. - Eur. J.* **2014**, *20*, 11283.
[7] R.-z. Zhang, X.-y. Hu, P. Guo, C.-l. Wang, *Phys. B* **2012**, *407*, 1114.
[8] T. Wu, P. Gao, *Materials (Basel)* **2018**, *11*, 999.
[9] R. A. Tomofumi YAMADA, Y. Takeshi, G. Manabu, *J. Ceram. Soc. Jpn.* **2013**, *121*, 706.
[10] C. Mallada, J. L. Menéndez, O. J. Dura, M. A. López de la Torre, R. Menéndez, R. Santamaría, *J. Eur. Ceram. Soc.* **2017**, *37*, 3741.
[11] X. Xiao, M. Widenmeyer, W. Xie, T. Zou, S. Yoon, M. Scavini, S. Checchia, Z. Zhong, P. Hansmann, S. Kilper, A. Kovalevsky, A. Weidenkaff, *Phys. Chem. Chem. Phys.* **2017**, *19*, 13469.
[12] H. Muta, K. Kurosaki, S. Yamanaka, *J. Alloys Compd.* **2004**, *368*, 22.
[13] H. Anno, K. Yamaguchi, T. Nakabayashi, H. Kurokawa, F. Akagi, M. Hojo, N. Toshima, *IOP Conf. Ser.: Mater. Sci. Eng.* **2011**, *18*, 142003.
[14] J. Suchanicz, P. Czaja, K. Kluczewska, H. Czternastek, M. Sokolowski, A. Węgrzyn, *Phase Transitions* **2018**, *91*, 1036.
[15] P. Roy, V. Waghmare, T. Maiti, *RSC Adv.* **2016**, *6*, 54636.
[16] M. Nasir Khan, H. - T. Kim, H. Minami, H. Uwe, *Mater. Lett.* **2001**, *47*, 95.
[17] T. Kolodiazhnyi, A. Petric, M. Niewczas, C. Bridges, A. Safa-Sefat, J. E. Greedan, *Phys. Rev. B* **2003**, *68*, 085205.
[18] A. J. Ahmed, S. M. K. Nazrul Islam, R. Hossain, J. Kim, M. Kim, M. Billah, M. S. A. Hossain, Y. Yamauchi, X. Wang, *R. Soc. Open Sci.* **2019**, *6*, 190870.
[19] A. J. Ahmed, M. S. A. Hossain, S. M. K. Nazrul Islam, F. Yun, G. Yang, R. Hossain, A. Khan, J. Na, M. Eguchi, Y. Yamauchi, X. Wang, *ACS Appl. Mater. Interfaces* **2020**, *12*, 28057.

[20] F. Maglia, I. G. Tredici, U. Anselmi-Tamburini, *J. Eur. Ceram. Soc.* **2013**, *33*, 1045.
[21] S. Kaur, S. B. Narang, D. K. K. Randhawa, *J. Mater. Res.* **2017**, *32*, 1149.
[22] M. Sharafat Hossain, F. Al-Dirini, F. M. Hossain, E. Skafidas, *Sci. Rep.* **2015**, *5*, 11297.
[23] G. Romano, J. C. Grossman, *Appl. Phys. Lett.* **2014**, *105*, 033116.
[24] C.-S. Park, W. Han, D. I. Shim, H. H. Cho, H.-H. Park, *J. Electrochem. Soc.* **2016**, *163*, E155–E158.
[25] Y. Hudiono, A. Greenstein, C. Saha-Kuete, B. Olson, S. Graham, S. Nair, *J. Appl. Phys.* **2007**, *102*, 053523.
[26] K. D. Parrish, J. R. Abel, A. Jain, J. A. Malen, A. J. H. McGaughey, *J. Appl. Phys.* **2017**, *122*, 125101.
[27] H. Lee, D. Vashaee, D. Z. Wang, M. S. Dresselhaus, Z. F. Ren, G. Chen, *J. Appl. Phys.* **2010**, *107*, 094308.
[28] K. Park, J. S. Son, S. I. Woo, K. Shin, M.-W. Oh, S.-D. Park, T. Hyeon, *J. Mater. Chem. A* **2014**, *2*, 4217.
[29] S. Foster, M. Thesberg, N. Neophytou, *Phys. Rev. B* **2017**, *96*, 195425.
[30] L. R. d. S. Oliveira, V. Vargiamidis, N. Neophytou, *IEEE Trans. Nanotechnol.* **2019**, *18*, 896.
[31] J. C. Stewart, D. S. Matthew, J. P. Chris, J. H. Phil, I. J. P. Matt, R. Keith, C. P. Mike, *Z. Kristallogr. Cryst. Mater.* **2005**, *220*, 567.
[32] J. P. Perdew, K. Burke, M. Ernzerhof, *Phys. Rev. Lett.* **1996**, *77*, 3865.
[33] D. Shanno, *Math. Comput.* **1970**, *24*, 647.
[34] W. Luan, L. Gao, H. Kawaoka, T. Sekino, K. Niihara, *Ceram. Int.* **2004**, *30*, 405.
[35] S. Yoon, J. Dornseiffer, Y. Xiong, D. Grüner, Z. Shen, S. Iwaya, C. Pithan, R. Waser, *J. Eur. Ceram. Soc.* **2011**, *31*, 1723.

Editorial Office:
Wiley-VCH GmbH
Boschstraße 12, 69469 Weinheim
Germany
Tel.: (+49) 6201 606 125
Fax: (+49) 6201 606 510

Email: advelectronicmat@wiley.com

Reprint Order Form

Manuscript No.: _____
Customer No.: (if available) _____
Purchase Order No.: _____
Author: _____

Charges for Reprints in Euro (excl. VAT), prices are subject to change. Minimum order 50 copies.

No. of pages	50 copies	100 copies	150 copies	200 copies	300 copies	500 copies
1– 4	345,—	395,—	425,—	445,—	548,—	752,—
5– 8	490,—	573,—	608,—	636,—	784,—	1077,—
9–12	640,—	739,—	786,—	824,—	1016,—	1396,—
13–16	780,—	900,—	958,—	1004,—	1237,—	1701,—
17–20	930,—	1070,—	1138,—	1196,—	1489,—	2022,—
every additional 4 pages	147,—	169,—	175,—	188,—	231,—	315,—

Information regarding VAT: The charges for publication of *cover pictures /reprints/issues/poster/Video abstracts/* are considered to be "supply of services" and therefore subject to German VAT. However, if you are an institutional customer outside Germany, the tax can be waived if you provide us with the valid VAT number of your company. Non-EU customers may have a VAT number starting with "EU" instead of their country code, if they are registered with the EU tax authorities. If you do not have a valid EU VAT number and you are a taxable person doing business in a non-EU country, please provide a certification from your local tax authorities confirming that you are a taxable person under local tax law. Please note that the certification must confirm that you are a taxable person and are conducting an economic activity in your country. **Note:** certifications confirming that you are a tax-exempt legal body (non-profit organization, public body, school, political party, etc.) in your country do not exempt you from paying German VAT.

Please send me send bill me for

☐ no. of reprints

☐ high-resolution PDF file (330 Euro excl. VAT)
E-mail address: _____

❖ Special Offer:

If you order 200 or more reprints you will get a PDF file for half price.

Please note: It is not permitted to present the PDF file on the internet or on company homepages.

Cover Posters (prices excl. VAT)
Posters of published covers are available in two sizes:

☐ DinA2 42 x 60 cm / 17 x 24in (one copy: 39 Euro)

☐ DinA1 60 x 84 cm / 24 x 33in (one copy: 49 Euro)

Postage for shipping (prices excl. VAT)
overseas +25 Euro
within Europe +15 Euro

VAT number: _____

Mail reprints / copies of the issue to:

_____
_____
_____
_____
_____

Send bill to:

_____
_____
_____
_____

☐ **I will pay by bank transfer**

☐ **I will pay by credit card**

VISA, Mastercard and AMERICAN EXPRESS
For your security please use this link (Credit Card Token Generator) to create a secure code Credit Card Token and include this number in the form instead of the credit card data. Click here:
https://www.wiley-vch.de/editorial_production/index.php

CREDIT CARD TOKEN NUMBER

						V									

_____
Date, Signature

Wiley-VCH GmbH – A company of John Wiley & Sons, Inc. –
Location of the Company: Weinheim – Trade Register: Mannheim, HRB 736569
Managing Directors: Sabine Haag and Dr. Guido F. Herrmann